Design of OsII-based Sensitizers for Dye-Sensitized Solar Cells

This is the peer-reviewed version of the following article:

Robertson, N. (2013). Design of Os^{II}-based Sensitizers for Dye-Sensitized Solar Cells: Influence of Heterocyclic Ancillaries. *Chemsuschem*, 6(8), 1366–1375.

which has been published in final form at http://dx.doi.org/10.1002/cssc.201300417

Manuscript received: 03/05/2013; Article published: 10/07/2013

Design of Os^{II}-based sensitizers for dye-sensitized solar cells: Assessing the influence of heterocyclic ancillaries**

Fa-Chun Hu,[1] Sheng-Wei Wang,[1] Miquel Planells,[2] Neil Robertson,[2,*] Harihara Padhy,[1] Bo-Sian Du,[1] Yun Chi,[1,*] Po-Fan Yang,[3] Hao-Wu Lin,[3,*] Gene-Hsiang Lee,[4] Pi-Tai Chou[4,*]

[1]Department of Chemistry and Low Carbon Energy Research Center, National Tsing Hua University, Hsinchu 30013, Taiwan.

[2]EaStCHEM, School of Chemistry, Joseph Black Building, University of Edinburgh, West Mains Road, Edinburgh, EH9 3JJ, UK.

[3]Department of Materials Science and Engineering, National Tsing Hua University, Hsinchu 30013, Taiwan.

[4]Department of Chemistry, National Taiwan University, Taipei 10617, Taiwan.

[*]Corresponding authors; Y.C. e-mail: ychi@mx.nthu.edu.tw; N.R. e-mail: Neil.Robertson@ed.ac.uk; H.W.L. e-mail: hwlin@mx.nthu.edu.tw; P.T.C. e-mail: chop@ntu.edu.tw

[**]This research was supported by National Science Council of Taiwan under grants NSC 100-2119-M-002-008 and NSC-98-3114-E-007-005, and the UK EPSRC Global Grant EP/K004468 and APEX Grant EP/H040218.

Supporting information:
Supporting information for this article is available online at http://dx.doi.org/10.1002/cssc.201300417

Graphical abstract:

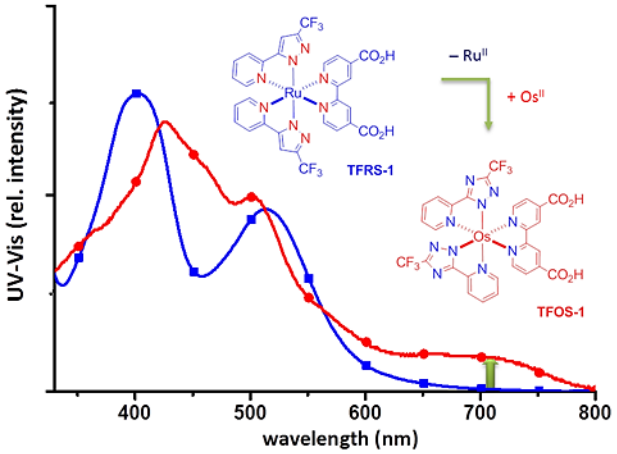

Keywords:
Osmium; triazole; N donor; dye sensitized solar cell; panchromatic.

Abstract

A series of new Os^{II} sensitizers (**TFOS-x**) with single 4,4'-dicarboxy-2,2'-dipyridine (H_2dcbpy) anchor and two chelating 2-pyridyl (or 2-pyrimidyl) triazolate ancillaries was successfully prepared. Single crystal X-ray structural analysis showed that their core geometry consists of one H_2dcbpy and two eclipsed and *cis*-arranged triazolate fragments, which is notably different from their Ru^{II} counterparts, in which the azolate (both pyrazolate and triazolate) fragments are located at the mutual trans-positions. Their basic properties were extensively probed using spectroscopic and electrochemical methods and TD-DFT calculation. Fabrication of dye sensitized solar cells (DSC) was then attempted using the I^-/I_3^- based solution electrolyte. One such DSC device using **TFOS-2** as the sensitizer showed promising performance characteristics of J_{SC} = 15.7 mA/cm^2, V_{OC} = 610 mV, FF = 0.63 and η = 6.08% under AM 1.5G simulated one-sun irradiation. Importantly, adequate IPCE performances were observed for all these **TFOS** derivatives over the wide spectral region of 450 to 950 nm, showing panchromatic light harvesting capability extended into the near infrared (NIR) regime. Our results thus underline a feasible strategy for maximizing J_{SC} as well as to reach the summit of DSC efficiency.

The pioneering work by Grätzel and coworkers has stimulated a surge of interest in the development of dye sensitized solar cells (DSCs) due to breakthroughs in the use of both Ru^{II} sensitizers and mesoporous TiO_2 photoelectrodes.[1] Later, a certified efficiency of 11.4% for the black dye,[2] and record high data of 11.5%, 11.3% and 11.7−12.1% were announced for respective CYC-B11,[3] C101,[4] and C106 dyes,[5] under illumination with standard AM 1.5G simulated sunlight. The outstanding performances of these Ru^{II} sensitizers are mainly attributed to their well extended absorption into the near infrared (NIR) regime. Recently quaterpyridine Ru^{II} sensitizers were also demonstrated with enhanced NIR absorption,[6] confirming their advantages in the aim to harvest lower energy photons.

Alternatively, Os^{II} based sensitizers seem to be a second option for satisfying these demands.[7] However, we must understand both the pros and cons of Os^{II} based materials before we can achieve the associated full advantages. First of all, Os^{II} polypyridine complexes have been shown to possess further red-shifted metal-to-ligand charge transfer (MLCT) transitions due to the lower oxidation potential of the Os^{II} metal element.[8] In addition, larger spin-orbit coupling for the heavier Os^{II} metal element will enhance the spin forbidden absorption;[9] thus, the Os^{II} sensitizers should display relatively more intense ^{3}MLCT absorption, together with the spin-allowed $^1\pi\pi^*$ and ^{1}MLCT transitions in the higher energy region. Such a combined advantage is pivotal to the development of panchromatic DSC cells with high proficiencies.

Conversely, the reduced oxidation potential of Os^{II} metal, vs. the second-row Ru^{II} counterpart, may render insufficient driving energy for dye regeneration by the I^-/I_3^- redox couple in standard electrolytes.[10] As a result, introduction of cyanide ancillary ligands[11] or employment of a cationic metal framework[12] have been undertaken to counterbalance the undesired electrochemical potentials. More recently, Chi and coworkers reported the Ru^{II} sensitizer **TF-2** with $E°_{ox}$ = 0.95 V vs. NHE, which possesses 4,4',4"-tricarboxy-2,2':6,2"-

terpyridine (H_3tctpy) and a functionalized dianionic 2,6-bis(1,2-pyrazol-5-yl) pyridine chelate, and confirmed that by replacing 2,6-bis(1,2-pyrazol-5-yl) pyridine with a more electron withdrawing 2,6-bis(1,2,4-triazol-5-yl) pyridine chelate, the respective Os^{II} sensitizer **TF-52** would display a similar potential of $E°_{ox}$ = 0.91 V, to maintain a comparable degree of electrochemical driving force for dye regeneration.[13] Accordingly, the DSC showed promising performance characteristics of J_{SC} = 23.3 mA/cm^2, V_{OC} = 600 mV, FF = 0.633 and η = 8.85% under AM 1.5G simulated one-sun irradiation, which remains the highest data recorded for Os^{II} based sensitizers.

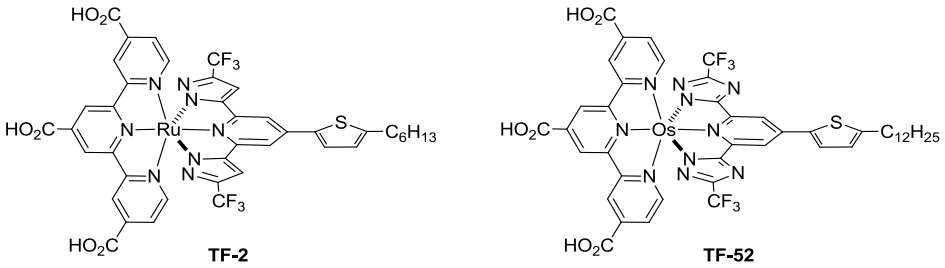

Scheme 1. Molecular structures of Ru^{II} and Os^{II} sensitizers **TF-2** and **TF-52**.

In the present article, we switch gear to tackle the alternative design of thiocyanate free Os^{II} sensitizers, namely: **TFOS-x**, x = 1, 2 and 3, with a single 4,4'-dicarboxy-2,2'-dipyridine (H_2dctbpy) anchor and two chelating 2-pyridyl (and 2-pyrimidyl) triazolate ancillaries. Since these Os^{II} based sensitizers are closely analogous to the class of Ru^{II} metal based **TFRS** sensitizers that were assembled using functionalized 2-pyridyl pyrazolate chelates,[14] we thus take this opportunity to assess both the basic design concept of thiocyanate-free architectures and the electronic as well as steric effects of the aforementioned chelating ancillaries in determining the sensitizers' performances. The collected knowledge will give valuable insight into the future modification of all classes of transition metal based DSC sensitizers.

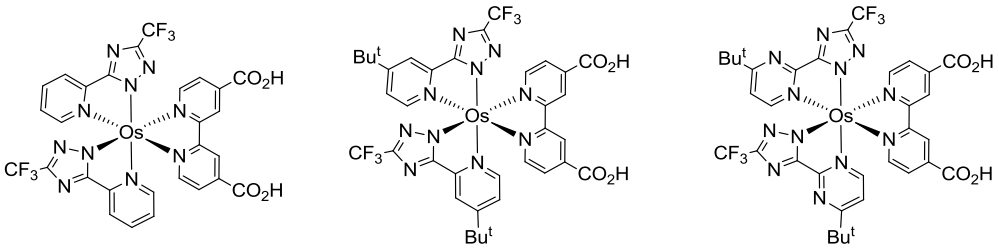

Scheme 2. Structural drawings of Os^{II} sensitizers under studied.

Results and discussion

Syntheses: To synthesize the proposed Os^{II} sensitizers, the required 2-pyridyl triazole chelates, (fptzH and fbpmtzH) were first prepared from the respective 2-cyanopyridine and NH_4Cl in methanol (for *in-situ* synthesis of pyridinecarboximidamide hydrochloride), followed by treatment with trifluoroacetic acid hydrazide to foster the formation of triazole; while the corresponding 2-pyrimidyl triazole chelate, 3-(trifluoromethyl)-5-(4-*t*-butyl-2-pyrimidyl)-1,2,4-triazole (fbpmtzH), was synthesized from 4-*tert*-butyl-2-cyanopyrimidine using the protocol described earlier.[15] The Os^{II} sensitizers were then obtained via a multistep procedure. First, 2-pyridyl (2-pyrimidyl) triazole was reacted with $Os_3(CO)_{12}$ in high boiling protic solvent, anhydrous diethylene glycol monoethyl ether (DGME). After this, DGME was removed *in vacuo* and replaced with nonpolar decalin as the next reaction solvent. After addition of diethyl 2,2'-bipyridine-4,4'-dicarboxylate (Et_2dcbpy), the resulting slurry was then heated at 190°C for 24 h to complete the synthesis of ethoxycarbonyl intermediates. This overall procedure, which is adopted and modified from that reported for synthesizing the relevant Os^{II} phosphors for organic light emitting diode (OLED) applications,[16] is in sharp contrast to the synthetic routes from cymene complex $[Ru(p\text{-cymeme})Cl_2]_2$ or even $RuCl_3$ hydrate used in the preparation of many Ru^{II} DSC sensitizers.

Structural characterization: In one case, the ethoxycarbonyl derivative, **TFOS-1-OEt**, was isolated and recrystallized for single crystal X-ray diffraction study to reveal and confirm the molecular structure. In all other cases, the ethoxycarbonyl intermediates were only purified by silica gel column chromatography, and next hydrolyzed in an alkaline solution of acetone and water for deprotection. Finally, the resulting Os^{II} sensitizers were precipitated from the solution by adjusting the pH to 3, followed by washing with diethylether and drying under vacuum. The typical yields run from 6% to 18%, which are calculated using $Os_3(CO)_{12}$ as the limiting reagent. Their purities were verified by routine mass, ^1H and ^{19}F NMR spectroscopies.

Figure 1 shows the ORTEP diagram of the ethoxycarbonyl intermediate **TFOS-1-OEt**, together with the selected bond distances and angles. As can be seen, the triazolate entities are located at the mutual *cis*-positions, which also results in the coordination sites opposite to the bipyridine anchor being occupied by a triazolate and pyridyl fragment from different ancillary chelates. If such a coordination configuration remains unchanged after hydrolysis, the structure will be different from all Ru^{II} based TFRS sensitizers documented, in which all azolate fragments (i.e. both pyrazolate and triazolate) maintain the mutual *trans*-dispositions and *cis*-arrangement with respect to the bipyridine anchor in the major isomer. [14] On the other hand, similar alternation of configuration for products has also been reported upon switching the group 8 metal reagents between $Os_3(CO)_{12}$ and $Ru_3(CO)_{12}$.[17] Apparently, this control of molecular configuration is not due to the steric origin of the ancillary chelates, but more plausibly to the electronic and intrinsic properties of the central metal atom.

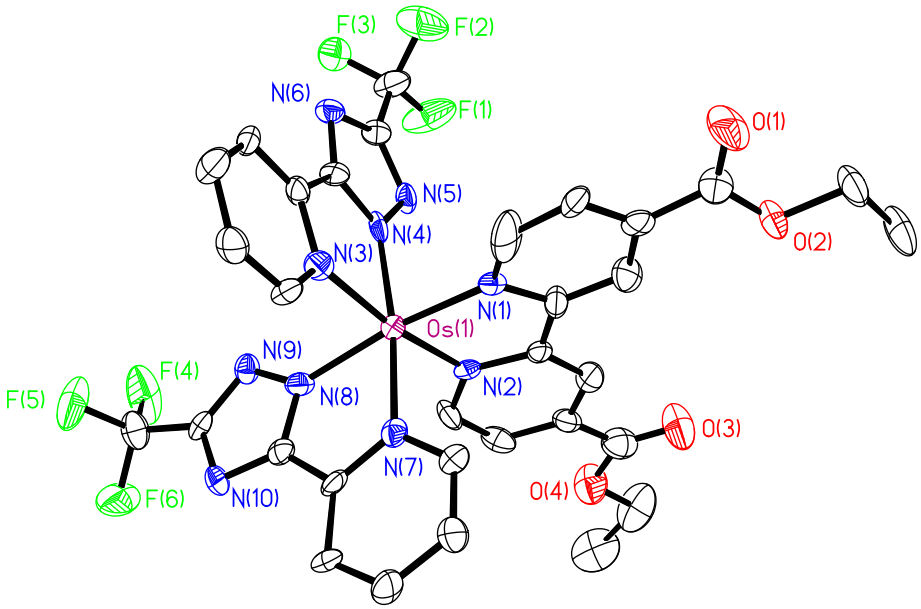

Figure 1. ORTEP diagram of complex **TFOS-1-OEt** (thermal ellipsoids shown at 50% probability level); selected bond lengths: Os-N(1) = 2.021(8), Os-N(2) = 2.031(9), Os-N(7) =2.087(9), Os-N(8) = 2.070(9), Os-N(3) = 2.095(9) and Os-N(4) =2.036(9) Å; selected bond angles: N(1)-Os-N(2) = 78.6(4), N(7)-Os-N(8) = 76.8(3), N(3)-Os-N(4) = 76.9(3), N(1)-Os-N(8) = 172.6(3), N(4)-Os-N(7) = 172.2(3), N(2)-Os-N(3) = 172.0(3)°.

Photophysical and electrochemical properties: The UV-Vis absorption spectra of the studied sensitizers, **TFOS-1** ~ **3** in DMF are depicted in Figure 2, together with the spectrum of the Ru^{II} sensitizer N719 reference. All pertinent numerical data are listed in Table 1. As can be seen, all three **TFOS** sensitizers showed dual metal-to-ligand charge transfer (MLCT) transitions at ~425 and 510 nm, and with molar absorption coefficients greater than 1.1×10^4 $mol^{-1}cm^{-1}$, which are more-or-less comparable to the MLCT bands observed in the N719 reference sensitizers. In addition, a broad shoulder around 703 ~ 741 nm (ε = ~2.1×10^3 $mol^{-1}cm^{-1}$) with the absorption on-set well extended into the NIR region of 800 nm was observed for all **TFOS** sensitizers. We attribute this broad peak to the spin-forbidden ^{3}MLCT absorption, for which the increased absorptivity is clearly the result of the enhanced spin-orbit coupling, induced by the heavy atom effect of the Os^{II} core.[9] In fact, many Os^{II} based phosphorescent emitters have shown such enhanced ^{3}MLCT absorption at the longer wavelength region of their UV/Vis spectra.[16] Furthermore, the red-shifting of ^{3}MLCT absorption for **TFOS-2** versus **1** is clearly attributed to the electron donating effect of the *t*-butyl substituent, which destabilizes the HOMO localized at the Os^{II} metal. In contrast, the blue-shifting of ^{3}MLCT

band of **TFOS-3** versus that of **TFOS-2** is caused by the electron withdrawing character of the pyrimidine versus pyridine fragments.

Dye	abs. λ_{max} [a] (nm) ($\times 10^3$ [$Lmol^{-1}cm^{-1}$])	Emission	Potentials and Energy levels		
		λ_{max} [a] (nm)	E_{ox} [b] (V)	$E_{0\text{-}0}$ [c] (V)	E_{ox}-$E_{0\text{-}0}$ (V)
TFOS-1	305 (20), 368 (8, sh), 428 (13), 505 (10), 713 (2.1)	834	0.71	1.67	-0.96
TFOS-2	306 (20), 424 (15), 516 (11), 741 (2.1)	845	0.69	1.60	-0.91
TFOS-3	305 (18), 370 (9, sh), 429 (14), 494 (11), 703 (2.1)	807	0.77	1.67	-0.90

[a] Absorption and emission spectra were measured in DMF solution.

[b] Oxidation potential of dyes was measured in DMF with 0.1 M [TBA][PF_6] and with a scan rate of 50 mVs^{-1}. It was calibrated with Fc/Fc^+ as internal reference and converted to NHE by addition of 0.63 V.

[c] $E_{0\text{-}0}$ was determined from the intersection of the absorption and tangent of the emission peak in DMF.

Table 1. Photophysical and electrochemical data of the studied **TFOS** sensitizers.

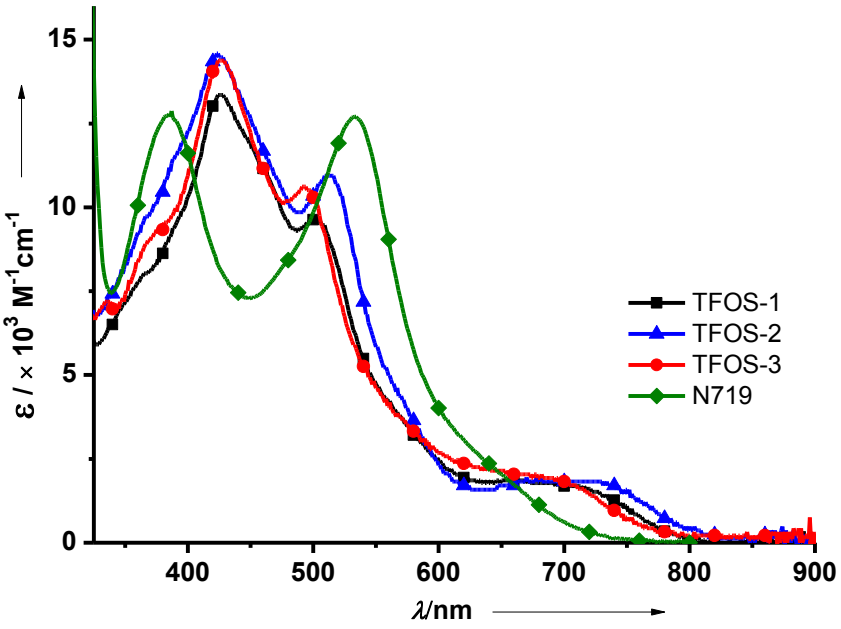

Figure 2. UV-Vis absorption spectra of **TFOS** sensitizers in DMF (1×10^{-5} M).

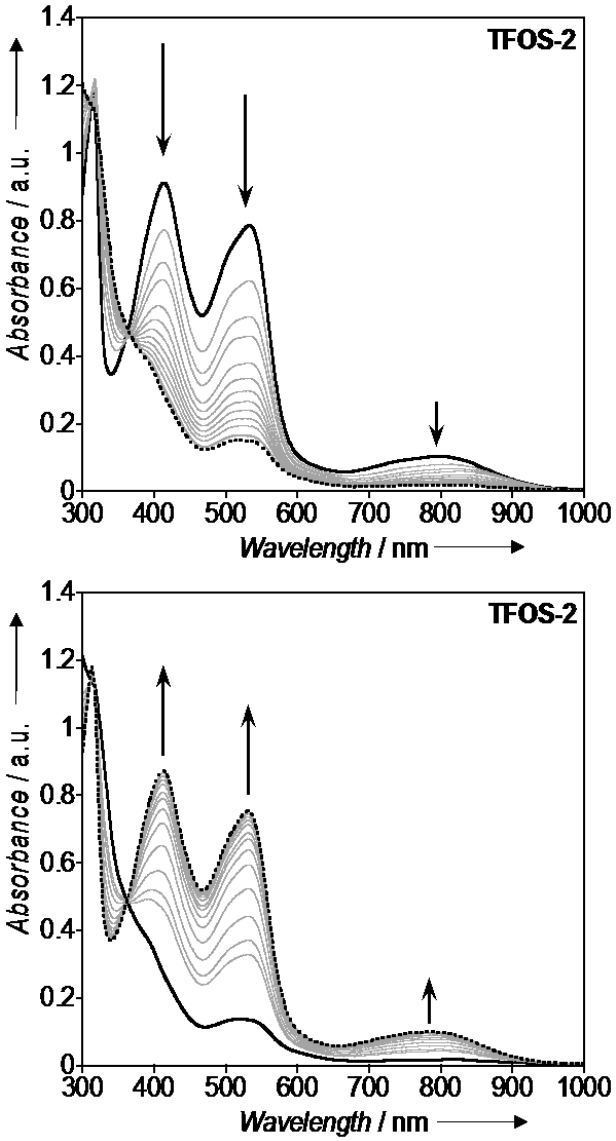

Figure 3. Spectroelectrochemistry of **TFOS-2** in 0.1 M [TBA][PF_6] DMF solution at 263 K after applying +0.9 V (*top*) and re-reducing by applying +0.2 V (*bottom*). Initial (*solid line*) and final (*dashed line*) states are marked.

Cyclic voltammetry was then conducted to examine if the oxidation potentials of these **TFOS** sensitizers are suitably offset from the redox potential of I^-/I_3^- in the electrolyte. This is to ensure sufficient driving energy for dye regeneration and also to verify whether the excited state oxidation potential, $E°^*_{ox}$, is more negative than the conduction band of TiO_2 for efficient electron injection. Thus, the oxidation potentials were measured in DMF solution with 0.1 M (TBA)(PF_6) and a scan rate of 50 mVs^{-1} (*vs.* NHE). It was calibrated with Fc/Fc^+ as the reference and converted to NHE by addition of 0.63 V. As shown in Table 1, their electrochemical

oxidation potentials $E°_{ox}$ appeared in the range 0.77 − 0.71 V (vs. NHE), being marginally larger that of the I^-/I_3^- redox couple (ca. 0.4 V vs. NHE), but are less positive compared with the potential of the intermediate $I_2^{\bullet-}/I^-$ couple, ca. 0.79 ± 0.1 V (vs. NHE).[18] Alternatively, the oxidation potentials at the excited states $E°*_{ox}$ (−0.90 to −0.96 V), calculated using the equation $E°*_{ox} = E_{ox} - E_{0\text{-}0}$, for which $E_{0\text{-}0}$ is defined as the optical gap of the sensitizer, are sufficiently more negative than the conduction band edge of the TiO_2 electrode (ca. −0.5 V vs. NHE); the latter should imply favorable electron injection after photoexcitation.

UV/Vis/NIR spectroelectrochemistry of the **TFOS** sensitizers was also measured. As shown in Figure 2, after applying +0.9 V to **TFOS-2**, bands centered at 412, 531 and 795 nm decreased while a new band at 315 nm arose. An isosbestic point was clearly observed at 360 nm, confirming the unimolecular redox process. By applying a potential of +0.2 V the oxidized cation was re-reduced to the neutral species and thus the initial bands were fully recovered, showing another isosbestic point at 365 nm. The result demonstrates the full chemical and electrochemical reversibility of the dye oxidation which is significant for the DSC operation because dye degradation can lead to cell instability over time. For comparison, the N719 dye shows a chemically-irreversible oxidation under the same conditions, indicating the higher stability of the NCS-free, Os sensitizer. The spectroelectrochemical data of **TFOS-1** and **3** also showed similar spectral behavior compared with that of **TFOS-2**, for which the spectral data are depicted in Figures 1S and 2S of supporting information. We note that **TFOS-3** however, with 2-pyrimidyl triazolate ancillaries, showed a less chemically-reversible oxidation compared with **TFOS-1** and **2**. This fact suggests that the use of 2-pyrimidyl instead of 2-pyridyl moiety could have an undesirable effect on the process reversibility; nevertheless the oxidation was still more reversible than N719 under the same conditions.[19]

For all three complexes, by oxidizing the sensitizers (Os^{II} to Os^{III}) the two main bands in the visible (centered at approximately 410 and 520 nm) as well as the small band in the NIR (centered at approximately 800 nm) decreased. Fully oxidized Os^{III} complexes give only a small visible absorption band centered at 520 nm, with a much lower molar absorption coefficient than the neutral Os^{II} complexes. The reduced intensity of the visible and NIR bands is consistent with their assignment as MLCT processes and the oxidation process as Os^{II} centered. Note that a stronger band for oxidized Os^{III} complexes also appears at the UV region (320 nm), but it will not influence the photovoltaic performance since TiO_2 strongly absorbs in the UV region and the oxidized dye will be rapidly regenerated.

Computational studies: All three **TFOS** complexes showed very similar molecular orbital distribution. Table 2 shows the essential orbital distribution of **TFOS-2**, while those of **TFOS-1** and **3** are depicted in the supporting information (Table 1S). Among them, the HOMO–2 is mainly localised on the Os^{II} atom with strong *d* character. The HOMO–1 and HOMO are very close in energy (within 0.2 eV) and mainly localised on the Os^{II} atom (*d* character), although they show a small but significant contribution from the triazolate moiety (π character). On the other hand, the LUMO, LUMO+1 and LUMO+2 are mainly localised on the dcbpy ligand, having a strong π character. This feature is necessary for a good electron injection. Note that a

very small contribution from the Os^{II} atom can be seen for the LUMO and LUMO+1. The simulated spectra obtained by means of TD-DFT reproduced accurately the measured UV-Visible spectra for all three **TFOS** complexes (Table 2S in supporting information), showing two major bands in the visible region at approximately 400 and 490 nm, with a weaker band around 650 nm corresponding to a shoulder around 600 nm in the experimental spectra. Analysing their MO contribution shows a combination of HOMO–X to LUMO+X (where X = 0, 1 and 2) transitions, which in each case corresponds to a metal-to-ligand charge transfer (MLCT) band. The small band in the near-IR is not reproduced by the calculation, which was limited to the calculation of excited singlet transitions. Accordingly, this is consistent with assignment of the near-IR absorption to direct excitation to the MLCT triplet state.

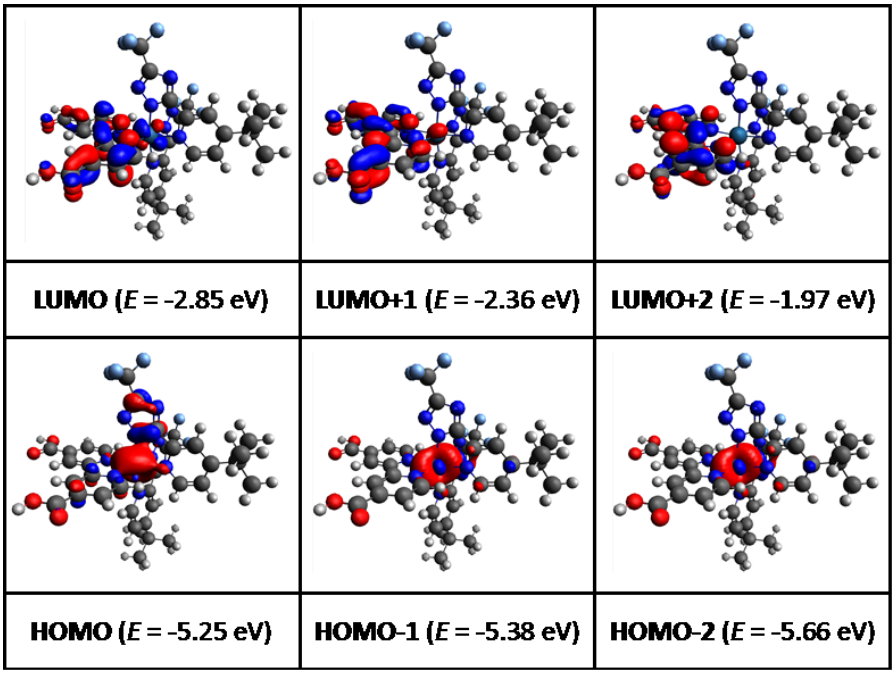

Table 2. Molecular orbital distributions of **TFOS-2** (isodensity = 0.04).

Performances of DSCs: The performance of the **TFOS** sensitizers in DSC devices was examined. The electrolyte composition of 0.6 M 1,2-dimethyl-3-propylimidazolium iodide (DMPII), 0.05 M iodine, 0.5 M *tert*-butylpyridine (TBP), and 0.1 M lithium iodide in acetonitrile, which is akin to that first reported for the **N749** sensitizer,[20] was applied to the DSC fabrication using **TFOS-1**. As can be seen in Table 3, this cell affords the parameters J_{SC} = 10.5 mA·cm^{-2}, V_{OC} = 580 mV and FF = 0.69, corresponding to an overall conversion efficiency η = 4.2 %. For further optimization, we then increased the concentration of LiI to 0.2 M, and combined with the concomitant increase of DMPII concentration to 1.0 M, such manipulations are expected to lower the TiO_2 conduction band potential and hence increase the rate of electron injection from

the excited sensitizers.[12b, 21] The final results are the notable improvement of the overall conversion efficiencies to η = 4.85 % (0.2 M LiI, 0.1 M DMPII) and 5.56 % (0.2 M LiI, 1.0 M DMPII).

Based on the optimized electrolyte composition (0.2 M LiI, 1.0 M DMPII) we then made further attempts to fabricate DSC using **TFOS-2** and **3** as the sensitizers. Also shown in Table 3, these two cells gave higher performance characteristics, i.e. J_{SC} = 15.7 mA·cm^{-2}, V_{OC} = 610 mV, FF = 0.63 and η = 6.08 % for **TFOS-2**, and J_{SC} = 15.6 mA·cm^{-2}, V_{OC} = 560 mV, FF = 0.69 and η = 6.00 % for **TFOS-3**. For a comparison, the efficiency for **N719** reference cell is recorded to be: J_{SC} = 18.9 mA·cm^{-2}, V_{OC} = 690 mV, FF = 0.70 and η = 9.18 %. This set of data shows the supremacy of Ru^{II} based sensitizer, despite that the **TFOS** sensitizers are capable to harvest solar irradiation down to the 950 nm regime. Among the optimized devices for **TFOS-x**, we attributed the increase of both J_{SC} and V_{OC} for **TFOS-2** versus those of **TFOS-1** to the inhibition of charge recombination, exerted by the bulky *t*-butyl substituents of **TFOS-2**.[22] In fact, there are many literature precedents that have shown the upward shifting of J_{SC} and V_{OC} by introducing steric demanding alkyl substituents on the sensitizers.[23] Furthermore, upon switching from pyridine to pyrimidine chelates, as showed in the pair of sensitizers **TFOS-2** and **-3**, the J_{SC} remains the same, whereas the V_{OC} dropped from 610 mV to 560 mV. This seems to be consistent with the increased charge recombination due to the pyrimidine fragments, which could exert a latent dative bonding between the uncoordinated pyrimidinyl nitrogen and iodine or triiodide in electrolyte solution.[24] Such interaction is expected to increase the local concentration of iodine or triiodide near the TiO_2 interface and hence the faster charge recombination.

Dye	EL	J_{sc} [mA cm^{-2}]	V_{oc} [mV]	FF	η [%]	Dye loading [× 10^{-7} mol cm^{-2}][d]
TFOS-1	[a]	10.5	580	0.69	4.20	-
	[b]	13.5	550	0.65	4.83	-
	[c]	14.1	590	0.67	5.56	1.58
TFOS-2	[c]	15.7	610	0.63	6.08	1.13
TFOS-3	[c]	15.6	560	0.69	6.00	1.28
N719	[c]	18.9	690	0.70	9.18	-

[a] Devices were fabricated using a 15+7 μm TiO_2 anode with printed area of 25 mm^2 and active area of 16 mm^2 defined by a shadow mask, while electrolyte consists of 0.6 M DMPII, 0.1 M LiI, 0.05 M I_2 and 0.5 M tBP in acetonitrile.

[b] The electrolyte with conc. of LiI increased to 0.2 M. [c] Electrolyte with conc. of LiI and DMPII being increased to 0.2 M and 1.0 M.

[c] The dye loading on 15+7 μm TiO_2 films was desorbed in 0.1 M of TBAOH in 1:1 (*v/v*) mixture of MeOH and H_2O and then estimated using the UV/Vis spectral analysis.

Table 3. The performances for DSCs measured under AM 1.5G one sun irradiation.[a]

The incident photon-to-current conversion efficiencies (IPCEs) using these DSC dyes are shown in Figure 4. The steep rise of the IPCE action spectra starts at 850 ~ 900 nm, showing their panchromatic absorption character. Adequate IPCE performances were then observed over the wide spectral region of 450 to 850 nm. The first IPCE maximum of ~60% was observed at 550 nm for all cells, followed by a local minimum at ~650 nm and a second IPCE maximum upon reaching ~790 nm. The minimum and the second maximum of the IPCE spectra seem to correlate well with the absorption minimum and the lowest energy MLCT maximum observed in the absorption spectra (Figure 2). However, the IPCE performance of the MLCT band seems to be much superior to that of the higher energy one. This can be confirmed by the notable increase of relative IPCE value at 790 and 550 nm of **TFOS-2** (i.e. 44% ÷ 62% = 0.71), versus the difference in molar extinction coefficient of the bands at 741 and 516 nm (i.e. 2100 ÷ 11000 = 0.19), showing a clear enhancement of electron collection capability for the lowest energy MLCT band.[25] Unfortunately, increasing the TiO_2 thickness (i.e. 18+5 μm) failed to improve the IPCE performances of these **TFOS** sensitizers.

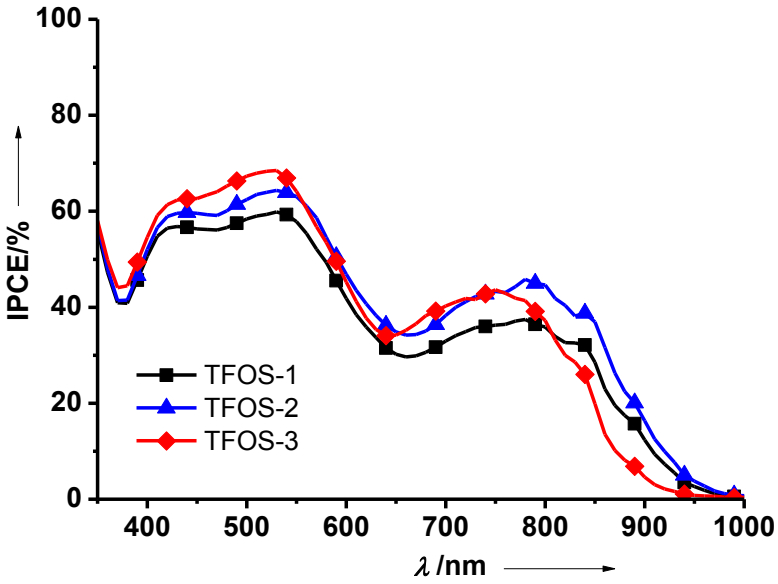

Figure 4. IPCE spectra for DSSCs sensitized with various Os^{II} based dyes.

Figure 5 shows the photocurrent density-voltage curves of the DSC devices recorded under AM1.5 G simulated sunlight at a light intensity of 100 $mWcm^{-2}$. **TFOS-2** showed the best data among all the sensitizers. Although its conversion efficiency is lower than that of the best Os^{II} based sensitizer TF-52 (8.85 %),[13b] **TFOS-2** remains comparable and superior to the Os^{II} sensitizers recently reported by Segawa (6.1%)[12d] and by Arakawa (2.7 %)[12c]. It is notable that our best J_{SC} obtained (15.7 $mA \cdot cm^{-2}$) is nevertheless

lower than the precedent for this class of Os^{II} sensitizers (J_{SC} = 18.8 ~ 23.3 mA·cm^{-2}). Thus, future optimization relies on how to improve the J_{SC} without simultaneously degrading V_{OC}.

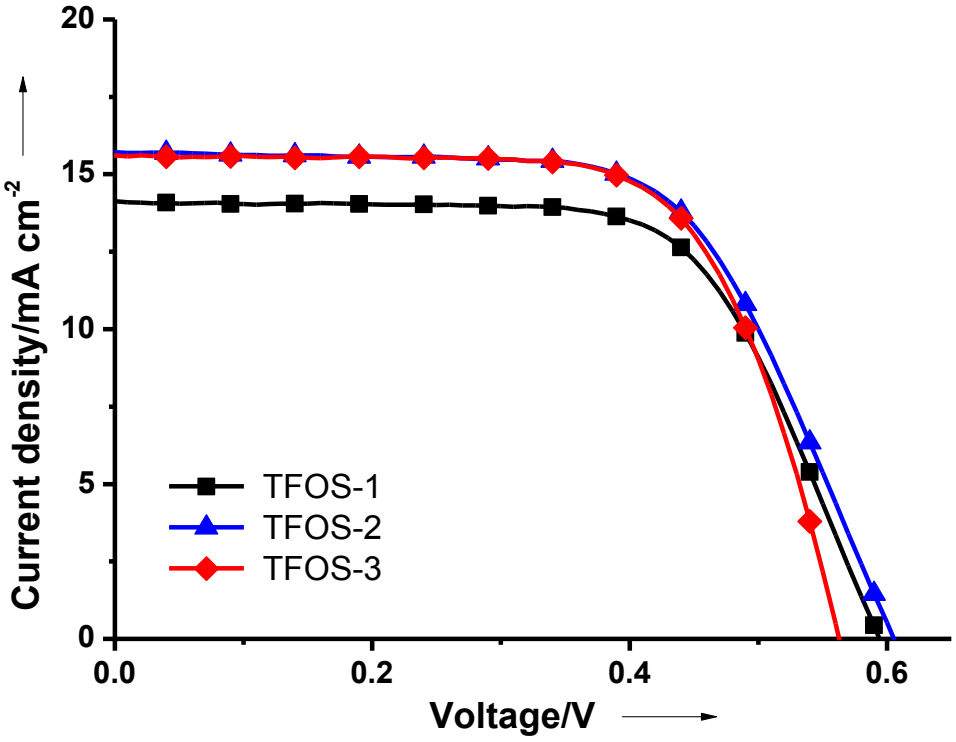

Figure 5. *J-V* characteristics measured under AM1.5 condition for DSSCs sensitized with various **TFOS** sensitizers.

To understand the different V_{OC} values for the DSCs, electrochemical impedance spectroscopy (EIS)[26] and transient photocurrent (TPC) and transient photovoltage (TPV) measurements were conducted.[27] EIS is a powerful tool for investigating electronic and ionic transport processes in DSCs, which provides valuable information for the understanding of photovoltaic parameters. TPV is used to study the amount of charge in a device under illumination. TPC measures the lifetime of electrons in devices under operational conditions and therefore recombination lifetime.

Previous studies have reported that two important factors affect V_{OC}: (1) TiO_2 conduction band edge movement with respect to the redox electrolyte energy and (2) photovoltage loss due to recombination at the TiO_2/electrolyte interface.[28] We performed TPV and TPC measurements to extract these data.[29] As shown in Figure 6(a) the **TFOS-1** device exhibits a higher V_{OC} at a fixed photo-induced charge density due to an

upward shift of the band edges compared to **TFOS-2** and **3**. However, to fully explain the trend of device V_{OC} under illumination, electron recombination needs to be taken into account as well.

Accordingly, as depicted in Figure 6b, the relative electron lifetime follows a distinctive order **TFOS-2** > **1** > **3**. This trend can be understood by the presence of bulky *t*-butyl group on the ancillary chelates of **2** versus that of **1**, which then reduced the electron recombination at the TiO_2-electrolyte interface. On the other hand, **TFOS-3** possesses uncoordinated nitrogen atom on the pyrimidinyl ancillaries versus those of both **1** and **2**. In such case, these nitrogen atoms could interact with the I_2 (or I_3^-),[24] and hence increase the back electron transfer, giving the lowest electron lifetime.

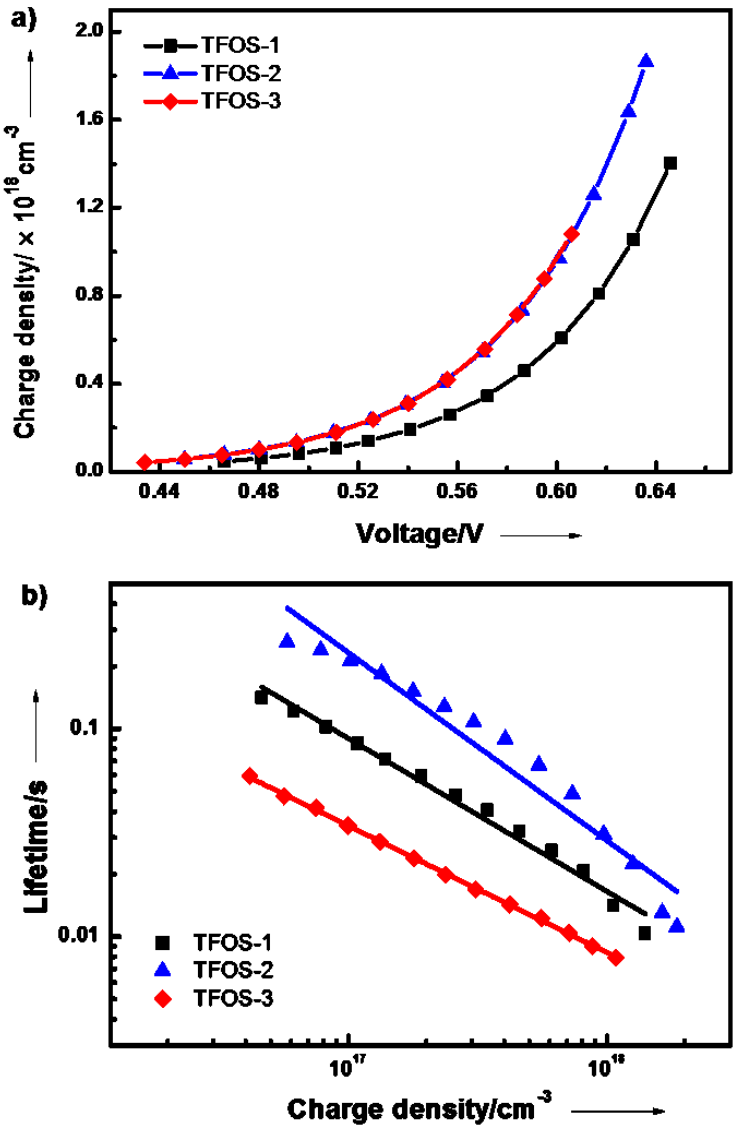

Figure 6. a) TiO_2 electron density versus voltage deduced from TPC measurements and b) electron lifetime τ versus TiO_2 electron density deduced from TPV measurements for DSC devices containing **TFOS** sensitizers. The cell voltage is induced via illumination from a variable intensity halogen lamp.

Figure 7 shows the Nyquist plots measured under dark conditions at a forward bias of various V_{OC}. The high frequency arc is due to the resistance and capacitance at the platinum counter electrode, the intermediate frequency arc is the recombination resistance (R_{rec}) associated with electron recombination at the interface, combined with the chemical capacitance (C_{μ}) of electrons in TiO_2, and the low frequency arc is attributed to the impedance of diffusion of redox species in the electrolyte.[30] The radii of the second semicircles indicate R_{rec} to be in the order of **TFOS-2** > **1** >> **3**. A smaller R_{rec} value in theory means faster charge recombination between electrons in TiO_2 and electron acceptors in the electrolyte and thus shorter TiO_2 electron lifetimes. The results are consistent with the electron lifetimes measured by TPV/TPC (see Figure 6) which is coincident with the trend in device V_{OC}. The results suggest that carrier recombination is the dominant factor to determine device V_{OC} in the **TFOS** dyes.

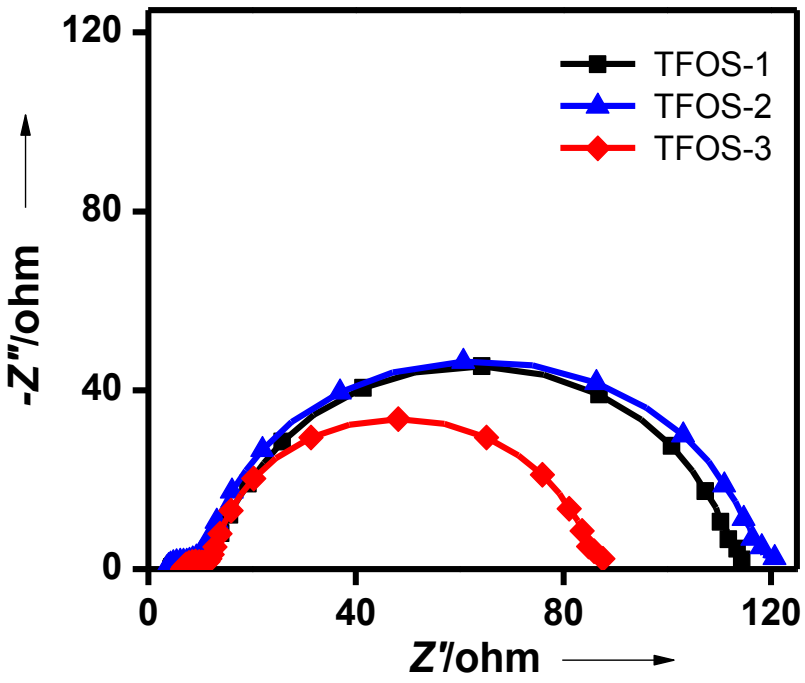

Figure 7. Nyquist plots measured under dark at a forward bias of corresponding open circuit voltage for the DSCs employing different **TFOS** sensitizers.

Conclusion

In summary, 2-pyridyl and 2-pyrimidinyl 1,2,4-triazole ancillary chelates were successfully incorporated to the coordination sphere of Os^{II} metal, affording three new Os^{II} based thiocyanate-free DSC sensitizers. We

also demonstrate that these Os^{II} complexes are suitable dyes to fabricate DSCs using the I^-/I_3^- electrolyte solution, and achieved the cell performances of J_{SC} = 15.7 mA/cm^2, V_{OC} = 610 mV, FF = 0.63 and η = 6.08% for **TFOS-2** under AM 1.5G simulated one-sun irradiation. DFT calculation shows that their HOMOs are mainly localized at the Os^{II} metal and partially on the axial substituted triazolate fragment, while the LUMOs are dominated by the unique dcbpy anchor. This feature is necessary for a good electron injection upon photoexcitation. Moreover, one practical advantage is their panchromatic light harvesting capability extended into near infrared (NIR) of around 950 nm, achieved by simple replacement of Ru^{II} with more reducible and heavier Os^{II} metal. Our results thus underline an attainable strategy for maximizing J_{SC} of DSCs with potential industrial applications.

Experimental section

General procedures: All reactions were performed under nitrogen. Solvents were distilled from appropriate drying agents prior to use. Commercially available reagents were used without further purification. Synthesis of 4-*tert*-butyl-2-cyanopyrimidine (L2-2) was achieved by direct cyanation of 4-*tert*-butyl-2-chloropyrimidine, which was synthesized by treatment of 2,4-dichloropyrimidine with *tert*-butylmagnesium chloride in the presence of cuprous iodide as catalyst.[31] The obtained 2-cyanopyrimidine was then converted to 3-(trifluoromethyl)-5-(4-*tert*-butyl-2-pyrimidyl)-1,2,4-triazole (L2) according to a literature method.[32] All reactions were monitored by TLC with pre-coated silica gel plates (Merck, 0.20 mm with fluorescent indicator UV254). Compounds were visualized with UV irradiation at 254 or 365 nm. Flash column chromatography was carried out using silica gel obtained from Merck (230-400 mesh). Mass spectra were obtained on a JEOL SX-102A instrument operating in electron impact (EI) or fast atom bombardment (FAB) mode. ^{1}H, and ^{19}F NMR spectra were recorded on a Bruker-400 or INOVA-500 instrument; chemical shifts are quoted with respect to the internal standard tetramethylsilane. Photophysical data were obtained using an Edinburgh Fluorescence spectrometer FLS928P.

Synthesis of TFOS-1: 3-(Trifluoromethyl)-5-(2-pyridyl)-1,2,4-triazole (fptzH, 298 mg, 1.39 mmol) and $Os_3(CO)_{12}$ (200 mg, 0.22 mmol) were dissolved in DGME (30mL), and the reaction mixture was heated to 180 °C for 24 h. After cooling to RT, a freshly prepared DGME solution of Me_3NO (104 mg, 1.39 mmol) was slowly added into the reaction mixture and the solution was heated at 110 °C for 1 h. After cooling, all volatile components were removed *in vacuo*, and then diethyl 2,2'-bipyridine-4,4'-dicarboxylate (dcbpy, 208 mg, 0.69 mmol) and decalin (30mL) were added into the flask and the mixture was then heated at 190°C for another 24 h. Finally, the solvent was removed under vacuum to afford a tardy residue, which was purified by silica gel column chromatography eluting with ethyl acetate. Recrystallization was then conducted in a CH_2Cl_2 / hexane mixture to give a dark-brown solid $Os(fptz)_2(Et_2dcbpy)$ (**TFOS-1-OEt**, 190 mg, 31%).

For hydrolysis, the resulting solid (**TFOS-1-OEt**, 67 mg, 0.07 mmol) was dissolved in a mixture of acetone (5 mL) and 2 M NaOH solution (0.73 mL, 1.46 mmol). The solution was heated to reflux for 12 h. After then, the solvent was removed and the residue was dissolved in water and titrated with 2 N HCl to pH 3 to afford a brown precipitate. This brown precipitate was washed with acetone and ether in sequence, giving dark-brown $Os(fptz)_2(H_2dcbpy)$ (**TFOS-1**, 40 mg, 64%).

Spectra data of **TFOS-1-OEt**: MS (FAB, ^{192}Os): *m/z* 918 [M^+]; ^1H NMR (400 MHz, [D_6] acetone, 25 °C): δ = 8.98 (d, ^3J(H,H) = 7.2 Hz, 2H; CH_2), 8.35 (d, ^3J(H,H) = 6.2 Hz, 1H; CH), 8.17 (d, ^3J(H,H) = 6.1 Hz, 1H; CH), 8.12 (t, ^3J(H,H) = 7.2 Hz, 2H; CH_2), 7.85 (t, ^3J(H,H) = 7.8 Hz, 1H; CH), 7.80 (t, ^3J(H,H) = 7.8 Hz, 1H; CH), 7.68 (d, ^3J(H,H) = 5.7 Hz, 1H; CH), 7.61 (d, ^3J(H,H) = 5.8 Hz, 2H; CH_2), 7.56 (d, ^3J(H,H) = 6.0 Hz, 1H; CH), 7.27 (t, ^3J(H,H) = 6.7 Hz, 1H; CH), 7.16 (t, ^3J(H,H) = 6.8 Hz, 1H; CH), 4.41 (q, ^3J(H,H) = 6.8 Hz, 4H; $2CH_2$), 1.38 ppm(q, ^3J(H,H) = 6.6 Hz, 6H; $2CH_3$). ^{19}F-{^1H} NMR (376 MHz, [D_6] acetone, 25 °C): δ = -63.70 (s, 3F; CF_3), -63.78 ppm (s, 3F; CF_3).

Selected structural data of **TFOS-1-OEt**: $C_{32.5}H_{26}ClF_6N_{10}O_{4.5}Os$; M = 968.28; triclinic; space group = $P\bar{1}$; a = 13.8555(10) Å, b = 15.3242(11) Å, c = 17.8112(12) Å, α = 83.389(2)°, β = 89.451(2)°, γ = 70.689(2)°, V = 3543.6(4) $Å^3$; Z = 4; ρ_{calcd} = 1.185 $Mg \cdot m^{-3}$; F(000) = 1896; crystal size = 0.15 × 0.08 × 0.05 mm^3; λ(Mo-K_α) = 0.71073 Å; T = 150(2) K; μ = 3.761 mm^{-1}; 24869 reflections collected, 12489 independent reflections (R_{int} = 0.0861), data / restraints / parameters = 12489 / 48 / 1005, GOF = 1.052, final $R_1[I > 2\sigma(I)]$ = 0.0618 and wR_2(all data) = 0.1350; largest diff. peak and hole = 1.092 and -1.906 e.$Å^{-3}$.

Spectra data of **TFOS-1-OEt**: MS (FAB, ^{192}Os): *m/z* 918 [M^+]; ^1H NMR (400 MHz, [D_6] acetone, 25 °C): δ = 8.98 (d, ^3J(H,H) = 7.2 Hz, 2H; CH_2), 8.35 (d, ^3J(H,H) = 6.2 Hz, 1H; CH), 8.17 (d, ^3J(H,H) = 6.1 Hz, 1H; CH), 8.12 (t, ^3J(H,H) = 7.2 Hz, 2H; CH_2), 7.85 (t, ^3J(H,H) = 7.8 Hz, 1H; CH), 7.80 (t, ^3J(H,H) = 7.8 Hz, 1H; CH), 7.68 (d, ^3J(H,H) = 5.7 Hz, 1H; CH), 7.61 (d, ^3J(H,H) = 5.8 Hz, 2H; CH_2), 7.56 (d, ^3J(H,H) = 6.0 Hz, 1H; CH), 7.27 (t, ^3J(H,H) = 6.7 Hz, 1H; CH), 7.16 (t, ^3J(H,H) = 6.8 Hz, 1H; CH), 4.41 (q, ^3J(H,H) = 6.8 Hz, 4H; $2CH_2$), 1.38 ppm(q, ^3J(H,H) = 6.6 Hz, 6H; $2CH_3$). ^{19}F-{^1H} NMR (376 MHz, [D_6] acetone, 25 °C): δ = -63.70 (s, 3F; CF_3), -63.78 ppm (s, 3F; CF_3).

Synthesis of TFOS-2: A similar procedure was used as described for **TFOS-1**; the total yield, calculated using $Os_3(CO)_{12}$ as the limiting reagent, is around 8%.

Spectra data of **TFOS-2**: MS (FAB, ^{192}Os): *m/z* 973 [M^+]; ^1H NMR (400 MHz, [D_6] DMSO, 25 °C): δ = 8.96 (d, ^3J(H,H) = 5.6 Hz, 2H; CH_2), 8.05 (d, ^3J(H,H) = 5.6 Hz, 2H; CH_2), 8.01 (s, 1H; CH), 7.97 (d, ^3J(H,H) = 6.0 Hz, 1H; CH), 7.62 (dd, ^3J(H,H) = 6.0, ^4J(H,H) = 1.6 Hz, 1H; CH), 7.58 (dd, ^3J(H,H) = 6.4, ^4J(H,H) = 1.6 Hz, 1H; CH), 7.40 (dd, ^3J(H,H) = 6.0, ^4J(H,H) = 2.4 Hz, 1H; CH), 7.32 (d, ^3J(H,H) = 6.2 Hz, 1H; CH), 7.25 (s, 2H; CH_2), 1.33 (s, 9H; $3CH_3$), 1.28 ppm (s, 9H; $3CH_3$). ^{19}F-{^1H} NMR (376 MHz, [D_6] DMSO, 25 °C): δ = -61.77 (s, 3F; CF_3), -61.96 ppm (s, 3F; CF_3).

Synthesis of TFOS-3: A similar procedure was used as described for **TFOS-1**; the total yield, calculated using $Os_3(CO)_{12}$ as the limiting reagent, is around 6%.

Spectra data of **TFOS-3**: MS (FAB, ^{192}Os): *m*/*z* 976 [M^+]; ^1H NMR (400 MHz, [D_6] DMSO, 25 ^oC): δ = 9.02 (d, ^3J(H,H) = 5.6 Hz, 2H; CH_2), 8.25 (d, ^3J(H,H) = 6.2 Hz, 1H; CH), 7.97 (d, ^3J(H,H) = 6.1 Hz, 1H; CH), 7.91 (d, ^3J(H,H) = 6.2 Hz, 1H; CH), 7.69 (d, ^3J(H,H) = 6.1 Hz, 1H; CH), 7.62 ~ 7.58 (m, 2H; CH_2), 7.40 (d, ^3J(H,H) = 6.2 Hz, 1H; CH), 7.27 (d, ^3J(H,H) = 6.2 Hz, 1H; CH), 1.37 (s, 9H; $3CH_3$), 1.32 ppm (s, 9H; $3CH_3$). ^{19}F-{^1H} NMR (376 MHz, [D_6] DMSO, 25 ^oC): δ = -62.01 (s, 3F; CF_3), -62.11 ppm (s, 3F; CF_3).

X-ray crystallography: All single-crystal X-ray diffraction data were measured on a Bruker Smart CCD diffractometer using λ (Mo Kα) radiation (λ = 0.71073 Å). The data collection was executed using the SMART program. Cell refinement and data reduction were made with the SAINT program. The structure was determined using the SHELXTL/PC program and refined using full matrix least-squares. All non-hydrogen atoms were refined anisotropically, whereas hydrogen atoms were placed at the calculated positions and included in the final stage of refinements with fixed parameters. CCDC-941062 contains the supplementary crystallographic data for this paper. These data can be obtained free of charge from the Cambridge Crystallographic Data Centre via www.ccdc.cam.ac.uk/data request/cif.

Spectroelectrochemistry: Spectroelectrochemical measurements were performed at 263 K by the optically transparent thin layer electrochemistry (OTTLE) technique in dry DMF containing 0.1 M [TBA][PF_6] supporting electrolyte using a 2 mm thick quartz cuvette. The conventional three-electrode electrochemical cell consisted of platinum gauze working electrode, platinum wire counter electrode and Ag/AgCl reference electrode (ferrocene $E_{1/2}$ = + 0.63 V). A potential of +0.9 V and +0.2 V was applied for the oxidation and re-reducing processes, respectively. The UV-Vis-NIR spectra were recorded with a Jasco V-670 spectrophotometer.

Computational details*:* The molecular structures were optimised in vacuum without any symmetry constrains, using the crystal structure provided as starting point geometry. The presence of a local minimum was confirmed by the absence of imaginary frequencies. All calculations were carried out using the Gaussian 09 program[33] with the Becke three parameter hybrid exchange, Lee Yang-Parr correlation functional (B3LYP) level of theory together with 6-31G(d) basis set for C, H, N, O and F atoms. The Os atom was treated with the SDD valence basis set and the MWB60 effective core potential.[34] All structures were input and processed through the Avogadro software package.[35] Time-dependent calculations (TD-DFT)[36] were performed using a long-range corrected functional CAM-B3LYP together with a more diffuse basis set 6-31+G(d) for non Os atoms using the previously optimised structure.[37] The 5 lowest singlet electronic transitions were calculated and processed with GaussSum software package.[38]

Device fabrication: The FTO glass used as current collector (4 mm thickness, Nippon Sheet Glass Co., Japan) was first cleaned with a detergent in an ultrasonic bath for 30 min, and then rinsed with water and ethanol.

After treatment in a UV-O_3 system for 15 min (PSD series UV-ozone cleaner, Novascan Technologies, Inc.), the FTO glass plates were immersed into a 40 mM aqueous $TiCl_4$ solution at 70 °C for 30 min and washed with water and ethanol. The nanocrystalline TiO_2 photoanodes were prepared using literature procedures. The TiO_2 electrodes of 15 μm thickness were deposited on transparent conducting glass, followed by deposition of a 7 μm scattering layer containing 400 nm TiO_2 particles (PST-400, JGC Catalysts and Chemicals, Japan). The working area is approx. 0.25 cm^2. The TiO_2 electrodes were heated under an air flow at 325 °C for 30 min, followed by heating at 375 °C for 5 min, 450 °C for 15 min, and 500 °C for 30 min. The TiO_2 electrodes were treated with a 40 mM aqueous solution of $TiCl_4$ and then sintered at 70 °C for 30 min and then washed with water and ethanol. The electrodes were heated again at 500 °C for 30 min and left to cool to 80 °C before dipping them into absolute ethanol with 25% (*v/v*) *t*-butanol for 18 h at 25 °C. The concentration of sensitizers was set to 0.1 mM, together with 0.2 mM of [TBA][DOC] and 10 mM of deoxycholic acid as co-adsorbate for suppressing aggregation. The Pt counter electrodes were prepared employing an H_2PtCl_6 solution (2 mg of Pt in 1 mL isopropyl alcohol) on FTO plates, followed by sintering at 400 °C for 15 min. The dye sensitized TiO_2 electrodes were assembled with Pt counter electrodes by inserting a hot-melt Surlyn film (Meltonix 1170-25, 25 μm, Solaronix) as spacer, and then heated at 130 °C. The electrolyte was then injected into the cell through a drilled hole at the counter electrode. Finally, the hole was sealed using a hot-melt Surlyn film and a cover glass. For measurement of PCE, a black metal mask of 0.16 cm^2 was employed to define the active area and to reduce scattered light from entering the solar cells.

Photovoltaic characterization: Photovoltaic measurements were tested under a Newport Oriel Class A Solar Simulator (Model 91159) equipped with a 150 W xenon light source. The output power density was calibrated to be 100 mW/cm^2 using a certificated KG-3 Si reference cell and with a circular aperture of 8 mm. The current-voltage characteristic of each cell was obtained with adopting 4-wire sense mode, delay time set as 100 ms and bias scan from short-circuit to open-circuit by using a Keithley digital source meter (Model 2400). The spectra of incident photon-to-current conversion efficiency (IPCE) were calculated with the equation of $1240 \cdot J_{SC}(\lambda)/(\lambda \cdot P_{in}(\lambda))$ where J_{SC} is the short-circuit current density under each monochromatic illumination in unit of A/cm^2, λ is the wavelength of incident monochromatic light in unit of nanometer, and P_{in} is the monochromatic light intensity in unit of W/cm^2 and were plotted as a function of incident wavelength with an increment of 10 nm. The current was pre-amplified by a current amplifier (SR570) and measured by Keithley 2400. It should be noted that 10 values of J_{SC} (interval 50 ms) were collected sequentially after a device was illuminated monochromatically 3 seconds later and were averaged for calculation of IPCE. A 300 W Xe lamp (Model 6258, Newport Oriel) combined with an Oriel cornerstone 260 1/4 m monochromator (Model 74100) provided a device under test with a monochromatic beam (dc mode). The beam power intensity was calibrated with a power meter (Model 1936-C, Newport) equipped with a Newport 818-UV photodetector.

Transient Photovoltage and Photocurrent Measurements: TPV and TPC measurements were taken using a Nd:YAG pumped dye laser (Rhodamine 6G) as an excitation source. A 100W variable intensity halogen lamp

was used as the bias light. Transient perturbations were amplified by a voltage/current preamplifier (Stanford Research System, SR560/SR570) and recorded by an oscilloscope (Tektronix). The electron lifetime and charge density could be extracted by the TPV and TPC data, respectively.[29]

Electrical Impedance Measurements: Electrical impedance experiments were carried out with a PARSTAT 2273 (AMETEK Princeton Applied Research, USA) electrochemical workstation, with a frequency range of $0.05 - 10^6$ Hz and a potential modulation of 10 mV at RT.

References

[1] a) M. Grätzel, *Nature* **2001**, *414*, 338-344; b) M. Grätzel, *Inorg. Chem.* **2005**, *44*, 6841-6851; c) M. Grätzel, *Acc. Chem. Res.* **2009**, *42*, 1788-1798.

[2] L. Han, A. Islam, H. Chen, C. Malapaka, B. Chiranjeevi, S. Zhang, X. Yang, M. Yanagida, *Energy Environ. Sci.* **2012**, *5*, 6057-6060.

[3] C.-Y. Chen, M. Wang, J.-Y. Li, N. Pootrakulchote, L. Alibabaei, C.-H. Ngoc-Le, J.-D. Decoppet, J.-H. Tsai, C. Grätzel, C.-G. Wu, S. M. Zakeeruddin, M. Grätzel, *ACS Nano* **2009**, *3*, 3103-3109.

[4] F. Gao, Y. Wang, D. Shi, J. Zhang, M. Wang, X. Jing, R. Humphry-Baker, P. Wang, S. M. Zakeeruddin, M. Grätzel, *J. Am. Chem. Soc.* **2008**, *130*, 10720-10728.

[5] Q. Yu, Y. Wang, Z. Yi, N. Zu, J. Zhang, M. Zhang, P. Wang, *ACS Nano* **2010**, *4*, 6032-6038.

[6] A. Abbotto, F. Sauvage, C. Barolo, F. De Angelis, S. Fantacci, M. Grätzel, N. Manfredi, C. Marinzi, M. K. Nazeeruddin, *Dalton Trans.* **2011**, *40*, 234-242.

[7] a) T. A. Heimer, C. A. Bignozzi, G. J. Meyer, *J. Phys. Chem.* **1993**, *97*, 11987-11994; b) M. Alebbi, C. A. Bignozzi, T. A. Heimer, G. M. Hasselmann, G. J. Meyer, *J. Phys. Chem. B* **1998**, *102*, 7577-7581.

[8] a) P.-T. Chou, Y. Chi, *Eur. J. Inorg. Chem.* **2006**, 3319-3332; b) Y. Chi, P.-T. Chou, *Chem. Soc. Rev.* **2007**, *36*, 1421-1431.

[9] S. Verma, P. Kar, A. Das, D. K. Palit, H. N. Ghosh, *Chem. Eur. J.* **2010**, *16*, 611-619.

[10] a) T. W. Hamann, J. W. Ondersma, *Energy Environ. Sci.* **2011**, *4*, 370-381; b) J. Cong, X. Yang, L. Kloo, L. Sun, *Energy Environ. Sci.* **2012**, *5*, 9180-9194; c) M. Wang, C. Grätzel, S. M. Zakeeruddin, M. Grätzel, *Energy Environ. Sci.* **2012**, *5*, 9394-9405.

[11] a) D. Kuciauskas, J. E. Monat, R. Villahermosa, H. B. Gray, N. S. Lewis, J. K. McCusker, *J. Phys. Chem. B* **2002**, *106*, 9347-9358; b) G. Sauve, M. E. Cass, G. Coia, S. J. Doig, I. Lauermann, K. E. Pomykal, N. S. Lewis, *J. Phys. Chem. B* **2000**, *104*, 6821-6836; c) R. Argazzi, G. Larramona, C. Contado, C. A. Bignozzi, *J. Photochem. Photobio. A* **2004**, *164*, 15-21.

[12] a) S. Altobello, R. Argazzi, S. Caramori, C. Contado, S. Da Fre, P. Rubino, C. Chone, G. Larramona, C. A. Bignozzi, *J. Am. Chem. Soc.* **2005**, *127*, 15342-15343; b) A. C. Onicha, F. N. Castellano, *J. Phys. Chem. C* **2010**, *114*, 6831-6840; c) T. Yamaguchi, T. Miyabe, T. Ono, H. Arakawa, *Chem. Commun.* **2010**, *46*, 5802-5804; d) T. Kinoshita, J.-i. Fujisawa, J. Nakazaki, S. Uchida, T. Kubo, H. Segawa, *J. Phys. Chem. Lett.* **2012**, *3*, 394-398.

[13] a) C.-C. Chou, K.-L. Wu, Y. Chi, W.-P. Hu, S. J. Yu, G.-H. Lee, C.-L. Lin, P.-T. Chou, *Angew. Chem. Int. Ed.* **2011**, *50*, 2054-2058; b) K.-L. Wu, S.-T. Ho, C.-C. Chou, Y.-C. Chang, H.-A. Pan, Y. Chi, P.-T. Chou, *Angew. Chem. Int. Ed.* **2012**, *51*, 5642-5646.

[14] a) K.-L. Wu, H.-C. Hsu, K. Chen, Y. Chi, M.-W. Chung, W.-H. Liu, P.-T. Chou, *Chem. Commun.* **2010**, *46*, 5124-5126; b) K.-L. Wu, W.-P. Ku, S.-W. Wang, A. Yella, Y. Chi, S.-H. Liu, P.-T. Chou, M. K. Nazeeruddin, M. Graetzel, *Adv. Funct. Mater.* **2013**, *23*, 2285-2294; c) S.-W. Wang, K.-L. Wu, E. Ghadiri, M. G. Lobello, S.-T. Ho, Y. Chi, J.-E. Moser, F. De Angelis, M. Grätzel, M. K. Nazeeruddin, *Chem. Sci.* **2013**, *4*, 2423-2433.

[15] P.-T. Chou, Y. Chi, *Chem. Eur. J.* **2007**, *13*, 380-395.

[16] a) B.-S. Du, J.-L. Liao, M.-H. Huang, C.-H. Lin, H.-W. Lin, Y. Chi, H.-A. Pan, G.-L. Fan, K.-T. Wong, G.-H. Lee, P.-T. Chou, *Adv. Funct. Mater.* **2012**, *22*, 3491-3499; b) S.-H. Chang, C.-F. Chang, J.-L. Liao, Y. Chi, D.-Y. Zhou, L.-S. Liao, T.-Y. Jiang, T.-P. Chou, E. Y. Li, G.-H. Lee, T.-Y. Kuo, P.-T. Chou, *Inorg. Chem.* **2013**, *52*, 5867-5875.

[17] P.-C. Wu, J.-K. Yu, Y.-H. Song, Y. Chi, P.-T. Chou, S.-M. Peng, G.-H. Lee, *Organometallics* **2003**, *22*, 4938-4946.

[18] a) S. Ardo, G. J. Meyer, *Chem. Soc. Rev.* **2009**, *38*, 115-164; b) G. Boschloo, E. A. Gibson, A. Hagfeldt, *J. Phys. Chem. Lett.* **2011**, *2*, 3016-3020.

[19] K. L. McCall, J. R. Jennings, H. Wang, A. Morandeira, L. M. Peter, J. R. Durrant, L. J. Yellowlees, J. D. Woollins, N. Robertson, *J. Photochem. Photobio. A* **2009**, *202*, 196-204.

[20] M. K. Nazeeruddin, P. Pechy, T. Renouard, S. M. Zakeeruddin, R. Humphry-Baker, P. Comte, P. Liska, L. Cevey, E. Costa, V. Shklover, L. Spiccia, G. B. Deacon, C. A. Bignozzi, M. Grätzel, *J. Am. Chem. Soc.* **2001**, *123*, 1613-1624.

[21] D. F. Watson, G. J. Meyer, *Coord. Chem. Rev.* **2004**, *248*, 1391-1406.

[22] K.-L. Wu, W.-P. Ku, J. N. Clifford, E. Palomares, S.-T. Ho, Y. Chi, S.-H. Liu, P.-T. Chou, M. K. Nazeeruddin, M. Grätzel, *Energy Environ. Sci.* **2013**, *6*, 859-870.

[23] a) C. Li, J.-H. Yum, S.-J. Moon, A. Herrmann, F. Eickemeyer, N. G. Pschirer, P. Erk, J. Schoeneboom, K. Muellen, M. Grätzel, M. K. Nazeeruddin, *ChemSusChem* **2008**, *1*, 615-618; b) J.-H. Yum, D. P. Hagberg, S.-J. Moon, K. M. Karlsson, T. Marinado, L. Sun, A. Hagfeldt, M. K. Nazeeruddin, M. Grätzel, *Angew. Chem. Int. Ed.* **2009**, *48*, 1576-1580; c) Y. Wu, X. Zhang, W. Li, Z.-S. Wang, H. Tian, W. Zhu, *Adv. Energy Mater.* **2012**, *2*, 149-156; d) M. Kimura, J. Masuo, Y. Tohata, K. Obuchi, N. Masaki, T. N.

Murakami, N. Koumura, K. Hara, A. Fukui, R. Yamanaka, S. Mori, *Chem. Eur. J.* **2013**, *19*, 1028-1034; e) Y. Cao, N. Cai, Y. Wang, R. Li, Y. Yuan, P. Wang, *Phys. Chem. Chem. Phys.* **2012**, *14*, 8282-8286.

[24] a) H. Kusama, H. Sugihara, *J. Photochem. Photobio. A* **2006**, *181*, 268-273; b) H. Kusama, M. Kurashige, H. Arakawa, *J. Photochem. Photobio. A* **2005**, *169*, 169-176.

[25] F. Gajardo, M. Barrera, R. Vargas, I. Crivelli, B. Loeb, *Inorg. Chem.* **2011**, *50*, 5910-5924.

[26] J. Bisquert, F. Fabregat-Santiago, I. Mora-Sero, G. Garcia-Belmonte, E. M. Barea, E. Palomares, *Inorg. Chim. Acta* **2008**, *361*, 684-698.

[27] a) D. Credgington, J. R. Durrant, *J. Phys. Chem. Lett.* **2012**, *3*, 1465-1478; b) P. R. F. Barnes, K. Miettunen, X. Li, A. Y. Anderson, T. Bessho, M. Grätzel, B. C. O'Regan, *Adv. Mater.* **2013**, *25*, 1881-1922.

[28] a) B. C. O'Regan, J. R. Durrant, *Acc. Chem. Res.* **2009**, *42*, 1799-1808; b) Z. Zhang, S. M. Zakeeruddin, B. C. O'Regan, R. Humphry-Baker, M. Grätzel, *J. Phys. Chem. B* **2005**, *109*, 21818-21824.

[29] a) B. C. O'Regan, S. Scully, A. C. Mayer, E. Palomares, J. Durrant, *J. Phys. Chem. B* **2005**, *109*, 4616-4623; b) H.-W. Lin, Y.-S. Wang, Z.-Y. Huang, Y.-M. Lin, C.-W. Chen, S.-H. Yang, K.-L. Wu, Y. Chi, S.-H. Liu, P.-T. Chou, *Phys. Chem. Chem. Phys.* **2012**, *14*, 14190-14195; c) H.-W. Lin, Y.-S. Wang, P.-F. Yang, K.-T. Wong, L.-Y. Lin, F. Lin, *Org. Electron.* **2013**, *14*, 1037-1044.

[30] a) S. M. Zakeeruddin, M. Grätzel, *Adv. Funct. Mater.* **2009**, *19*, 2187-2022; b) J. Halme, P. Vahermaa, K. Miettunen, P. Lund, *Adv. Mater.* **2010**, *22*, E210-E234; c) F. Fabregat-Santiago, J. Bisquert, G. Garcia-Belmonte, G. Boschloo, A. Hagfeldt, *Sol. Energy Mater. Sol. Cells* **2005**, *87*, 117-131.

[31] a) L. Hintermann, L. Xiao, A. Labonne, *Angew. Chem. Int. Ed.* **2008**, *47*, 8246-8250; b) J. M. Coteron, D. Catterick, J. Castro, M. J. Chaparro, B. Diaz, E. Fernandez, S. Ferrer, F. J. Gamo, M. Gordo, J. Gut, L. de las Heras, J. Legac, M. Marco, J. Miguel, V. Munoz, E. Porras, J. C. de la Rosa, J. R. Ruiz, E. Sandoval, P. Ventosa, P. J. Rosenthal, J. M. Fiandor, *J. Med. Chem.* **2010**, *53*, 6129-6152.

[32] S.-Y. Chang, J. Kavitha, S.-W. Li, C.-S. Hsu, Y. Chi, Y.-S. Yeh, P.-T. Chou, G.-H. Lee, A. J. Carty, Y.-T. Tao, C.-H. Chien, *Inorg. Chem.* **2006**, *45*, 137-146.

[33] M. J. Frisch, G. W. Trucks, H. B. Schlegel, G. E. Scuseria, M. A. Robb, J. R. Cheeseman, G. Scalmani, V. Barone, B. Mennucci, G. A. Petersson, H. Nakatsuji, M. Caricato, X. Li, H. P. Hratchian, A. F. Izmaylov, J. Bloino, G. Zheng, J. L. Sonnenberg, M. Hada, M. Ehara, K. Toyota, R. Fukuda, J. Hasegawa, M. Ishida, T. Nakajima, Y. Honda, O. Kitao, H. Nakai, T. Vreven, J. A. Montgomery, J. E. Peralta, F. Ogliaro, M. Bearpark, J. J. Heyd, E. Brothers, K. N. Kudin, V. N. Staroverov, R. Kobayashi, J. Normand, K. Raghavachari, A. Rendell, J. C. Burant, S. S. Iyengar, J. Tomasi, M. Cossi, N. Rega, J. M. Millam, M.

Klene, J. E. Knox, J. B. Cross, V. Bakken, C. Adamo, J. Jaramillo, R. Gomperts, R. E. Stratmann, O. Yazyev, A. J. Austin, R. Cammi, C. Pomelli, J. W. Ochterski, R. L. Martin, K. Morokuma, V. G. Zakrzewski, G. A. Voth, P. Salvador, J. J. Dannenberg, S. Dapprich, A. D. Daniels, Farkas, J. B. Foresman, J. V. Ortiz, J. Cioslowski, D. J. Fox, *Gaussian 09, Revision A.1; Gaussian Inc.* **2009**, Wallingford, CT.

[34] a) D. Andrae, U. Haeussermann, M. Dolg, H. Stoll, H. Preuss, *Theor. Chim. Acta* **1990**, *77*, 123-141; b) J. M. L. Martina, A. Sundermann, *J. Chem. Phys.* **2001**, *114*, 3408-3420.

[35] M. D. Hanwell, D. E. Curtis, D. C. Lonie, T. Vandermeersch, E. Zurek, G. R. Hutchison, *J. Cheminfor.* **2012**, *4*, 17.

[36] a) R. Bauernschmitt, R. Ahlrichs, *Chem. Phys. Lett.* **1996**, *256*, 454; b) D. J. Tozer, N. C. Handy, *J. Chem. Phys.* **1998**, *109*, 10180-10189.

[37] T. Yanai, D. P. Tew, N. C. Handy, *Chem. Phys. Lett.* **2004**, *393*, 51-57.

[38] N. M. O'boyle, A. L. Tenderholt, K. M. Langner, *J. Comp. Chem.* **2008**, *29*, 839-845.